Measuring electroweak quantum numbers of color sextet resonances at the LHC

Soubhik Kumar,[1,2,*] Rafiqul Rahaman,[3,†] and Ritesh K. Singh[4,‡]

[1]*Berkeley Center for Theoretical Physics, Department of Physics, University of California, Berkeley, California 94720, USA*
[2]*Theoretical Physics Group, Lawrence Berkeley National Laboratory, Berkeley, California 94720, USA*
[3]*Regional Centre for Accelerator-based Particle Physics, Harish-Chandra Research Institute, A CI of Homi Bhabha National Institute, Chhatnag Road, Jhunsi, Prayagraj 211019, India*
[4]*Department of Physical Sciences, Indian Institute of Science Education and Research Kolkata, Mohanpur 741246, India*

(Received 14 March 2023; revised 3 August 2023; accepted 22 August 2023; published 7 September 2023)

We study the prospect of measuring the electroweak quantum numbers of beyond the Standard Model color sextet particles that decay into same-sign top-quark pairs. Among these particles, the color sextet scalars give rise to top quarks with the same chirality, while the top quarks coming from the color sextet vector would have opposite chirality. This difference gets encoded in the angular distributions of the bottom quarks and leptons originating from the decays of the top quarks. We utilize this feature and the energy distributions of the final-state jets and leptons to distinguish among the three possible color sextet resonances, taking into account various SM background processes at the 13 TeV LHC.

DOI: 10.1103/PhysRevD.108.055006

I. INTRODUCTION

A variety of beyond the Standard Model (BSM) scenarios, especially those addressing the Higgs hierarchy problem, e.g., supersymmetry or composite Higgs, predict new physics around the TeV scale (see Ref. [1] for reviews). The search for such BSM states has been actively going on at the LHC and will continue through its high-luminosity (HL-LHC) phase, in conjunction with other indirect probes.

Given the absence of new physics at the LHC so far, we can ask a bottom-up and purely group theoretic question as follows. Noting that the Standard Model (SM) is based on the gauge group $SU(3)_c \times SU(2)_L \times U(1)_Y$, we can ask which possible BSM scalar or vector particles can have direct, tree-level couplings to SM fermions. *A priori*, there are a number of such BSM states [2,3]. However, a subset of them would couple to both leptons and quarks so as to mediate proton decay at tree level, unless that is forbidden by some other global symmetry, and therefore are ruled out [4] for TeV-scale masses. Among the remaining states, those coupling to two top quarks are particularly interesting from an experimental perspective. As we will discuss in the following, two such scalar and one such vector resonance have the SM quantum numbers,

$$\Phi_1 \sim (\mathbf{6}, \mathbf{1}, 4/3), \qquad \Phi_3 \sim (\mathbf{6}, \mathbf{3}, 1/3), \qquad \Phi_2^\mu \sim (\mathbf{6}, \mathbf{2}, 5/6). \tag{1}$$

At the LHC, these states can be produced via their couplings to the first-generation quarks, and subsequently, they can decay into a *like-sign* top-quark pair. The top quarks can then decay into a pair of b jets, a pair of like-sign leptons, and neutrinos when the intermediate W bosons decay leptonically. The phenomenology and ultraviolet origin of such color sextet diquarks have been discussed extensively in the literature; see, e.g., Refs. [2–16].

The question we would like to ask in the present work is the following: suppose a discovery of a color sextet particle is made at the (HL-)LHC. Then, purely based on the laboratory-frame observables, can we extract the quantum numbers of the discovered sextet state and distinguish among the three possible sets of quantum numbers of a generic color sextet particle, as mentioned in Eq. (1)?

To answer this, we first note that the fermionic couplings of interest are inherently chiral in nature. Therefore, the top quarks coming from the sextet decay would carry definite polarization, and this plays a crucial role in extracting the quantum numbers of the sextet states [12,14]. For example, the rest-frame angular distributions of leptons and b jets are

*soubhik@berkeley.edu
†rafiqulrahaman@hri.res.in
‡ritesh.singh@iiserkol.ac.in

different depending on the polarization of the parent top quarks, as we describe explicitly below. However, since in such processes the top quarks decay leptonically, there is missing energy in the form of neutrinos in the final state, and reconstructing the rest frame of a top quark is not immediate. While it is possible to use the M_{T2} observable [17,18] to address this issue [19,20], it is still useful to construct observables that do not rely on any such rest frame reconstruction. To this end, we construct some new laboratory-frame observables that can be used to investigate and isolate the quantum numbers of the various sextet states.

Some laboratory-frame observables for processes involving missing energy have been discussed in the literature. One example is the visible energy fraction of the leptons [21,22]

$$z_i = \frac{E_{l_i}}{E_{l_i} + E_{b_i}}. \tag{2}$$

Here, E_{l_i} and E_{b_i} are, respectively, the energies of the lepton and the associated b quark originating from the decay of the same top quark. This observable is sensitive to the polarization of the top quark. However, in the signal of our interest, we have two b jets and two leptons, and the effectiveness of z_i inherently depends on correctly pairing a b quark with the associated lepton. This motivates us to look for additional laboratory-frame observables which are independent of such pairing. We will show that such observables can be constructed based on the azimuthal distribution of final-state visible particles.

The rest of this work is organized as follows. In Sec. II, we describe the couplings of the sextet states to the SM fermions and the existing experimental constraints on such states. In Sec. III, we construct the laboratory-frame observables of interest and explain how top-quark polarization and spin correlation plays an important role in this context through a parton-level analysis at the 13 TeV LHC. In Sec. IV, we present our results to distinguish among the color sextet states through a detector-level simulation, taking into account possible SM backgrounds. We conclude in Sec. V.

II. MODEL

In this work, we focus on color sextet BSM resonances that couple to two top quarks. Given the quantum numbers of the SM quark doublet $q_L = \binom{u_L}{d_L} \sim (\mathbf{3}, \mathbf{2}, +1/6)$ and the right-handed up-type quark $u_R \sim (\mathbf{3}, \mathbf{1}, +2/3)$, the quantum numbers of the BSM scalar and vector resonances are fixed as in (1). We first consider the two scalars, Φ_1 and Φ_3. We can write the Yukawa coupling of Φ_1 as (see, e.g., Ref. [10])

$$\lambda_1 \bar{K}^a_{ij} \Phi_{1a} \bar{u}_{Ri} u^c_{Rj} + \text{H.c.}, \tag{3}$$

where the superscript c denotes charge conjugation operation. The matrices $\bar{K}^a_{ij}$ are determined by the Clebsch-Gordon coefficients for the sextet representation of $SU(3)$. In both Eqs. (3) and (4) below, the indices a and i, j correspond to color indices, and they run over $1 \cdots 6$ and $1 \cdots 3$, respectively.

The Yukawa coupling of Φ_3 is given in an analogous manner, except that it couples to the symmetric combination of two copies of q_L. The coupling to u_L is given by

$$\lambda_3 \bar{K}^a_{ij} \Phi_{3a} \bar{u}_{Li} u^c_{Lj} + \text{H.c.} \tag{4}$$

Here, we have focused on the part of the isospin triplet field that couples only to the up-type quarks since that can decay into a pair of top quarks, which is the signal of our interest. In both (3) and (4), we have suppressed the generation indices on the Yukawa couplings, λ_1 and λ_3.

Finally, the coupling of the vector resonance is described by

$$\lambda_2 \bar{K}^a_{ij} \Phi^\mu_{2,a} \bar{u}_{Rj} \gamma_\mu u^c_{Li} + \text{H.c.} \tag{5}$$

Here, we have focused on the up-quark coupling for the same reason as above. We will be agnostic about how Φ^μ_2 gets its mass.

For a general Yukawa coupling, there would be large flavor-changing neutral current processes mediated by the above sextet states. To avoid the stringent experimental constraints from those, we assume that the matrices λ_1, λ_2, and λ_3 are flavor diagonal.

With this assumption, the next stringent constraints on λ_1 come from the measurements of $D^0 - \bar{D}^0$ mixing [23],

$$\frac{|\text{Re}(\lambda_{1,cc}\lambda^*_{1,uu})|}{m^2_\phi} < x \times 7.2 \times 10^{-11}/\text{GeV}^2, \tag{6}$$

where $x = \Delta m_D/\Gamma_D$ is a $D^0 - \bar{D}^0$ mixing parameter. Assuming CP conservation and taking $x \approx 4 \times 10^{-3}$ [24], we get $\text{Re}(\lambda_{1,cc}\lambda^*_{1,uu}) < 3 \times 10^{-7}$ for $m_\phi = 1$ TeV. In the following, we will assume a hierarchy between $\lambda_{1,cc}$ and $\lambda_{1,uu}$ with $|\lambda_{1,cc}| \ll |\lambda_{1,uu}|$ so as to satisfy the above bound. The dominant constraints on λ_2 and λ_3 also come from $D^0 - \bar{D}^0$ mixing [12], which can again be suppressed by taking the couplings to second-generation quarks to be small as we mentioned above.

We note that Φ_1 and Φ_3 decay to a pair of right-handed and left-handed top quarks, respectively. This implies that we would be able to distinguish between the quantum numbers of these two sextet scalars using the polarization properties of the top quarks. In particular, in its rest frame, a right-handed top quark would decay into leptons whose average distribution would peak in the same direction as the top-quark spin, while the associated b-quark distribution would be peaked in the opposite direction. Thus, after

boosting to the laboratory frame, the angle between the two leptons, each coming from the two daughter top quarks from Φ_1 decay, will be peaked around $\Delta\phi = \pi$, while the angle between the two b quarks will be more broadly distributed around $\Delta\phi = \pi$. The situation with Φ_3 is exactly the opposite of this. While the vector BSM resonance Φ_2^μ decays into a same-sign top pair as well, the top quarks would have opposite chirality. These features can then be used to distinguish among Φ_1, Φ_2^μ, and Φ_3, as we will see below. We will refer to these particles as "singlet," "doublet," and "triplet," respectively, based on their $SU(2)_L$ quantum numbers. For numerical simulations, we choose the benchmark: $m_\phi = 1$ TeV, $\lambda_{uu} = \lambda_{tt} = 0.003$ for all three sextet particles. We note that there is an upper bound of 1.2 pb on the tt production cross section given by CMS coming from the same-sign dilepton, missing energy, and jets search [25]. However, the tt production cross sections in our models are much smaller compared to the CMS limit. For example, $\sigma_{tt} \simeq 0.02$ pb for the singlet case in our chosen benchmark, which is only 1% of the CMS limit.

III. OBSERVABLE

The polarization of a top quark is preserved in its decay products, and this plays an important role in our analysis. The double angular distribution of daughter fermions from the two top quarks can be expressed as [26]

$$\frac{1}{\sigma}\frac{d^2\sigma}{(d\cos\theta_1)(d\cos\theta_2)} = \frac{1}{4\pi}(1 + \alpha_1 p_{t_1}\cos\theta_1 + \alpha_2 p_{t_2}\cos\theta_2 + \alpha_1\alpha_2 p p_{tt}\cos\theta_1\cos\theta_2), \quad (7)$$

in terms of the polarization of two top quarks (p_{t_1}, p_{t_2}) and their spin correlation (pp_{tt}). Here, θ_i are the decay angles of the daughter fermions at their respective top quark's rest frame. The quantity α_i is called the analyzing power, which depends on the daughter fermion. For example, for a lepton, $\alpha_l = 1$, whereas for a b quark, $\alpha_b = -0.4$ [27]. The polarization p_t is positive (negative) for the right (left-)polarized top quark. The above formula in Eq. (7) is valid only in the rest frame of the top quark, which requires a complete reconstruction of the missing neutrinos [28–31]. The polarization of the top quark can also be obtained from the distribution of the ratio of energies of the daughter b quark (E_b) and the top quark (E_t), E_b/E_t. This again requires a complete reconstruction of the top-quark momenta and hence that of the neutrinos.

The visible energy fractions (z_i), as defined in Eq. (2), are correlated with the polarization of the top quarks and can let us distinguish between left and right chiral top quarks, without completely reconstructing their momenta. However, this requires a correct pairing of the two b quarks with the corresponding leptons. This can be achieved using the fact that in the laboratory frame a sibling lepton and a b quark have a smaller ΔR than the ΔR between a cousin lepton and a b quark. Here, $\Delta R = \sqrt{\Delta\phi^2 + \Delta\eta^2}$, where ϕ is the azimuthal angle and η is the pseudorapidity of a particle. We label the two leptons as l_1 and l_2, ordered according to their transverse momenta (p_T), i.e., with $p_T(l_1) > p_T(l_2)$. The two b quarks can pair with the leptons in two ways. If the correct pairs are such that l_1 and b_1 come from one top quark, while l_2 and b_2 come from another top quark, then we expect to have $\Delta R(l_1, b_1) + \Delta R(l_2, b_2) < \Delta R(l_1, b_2) + \Delta R(l_2, b_1)$. This criterion is satisfied for more than 96% of times for the chosen mass of 1 TeV. For a heavier scalar, the top quarks will be more boosted, which will lead their decay products to collimate further, and this increases the efficiency of pairing the lepton and the b quark correctly.

We study the distributions for the energy fraction variables z_1 and z_2 defined in Eq. (2), pairing the leptons and b quarks as described above using parton-level events at $\sqrt{s} = 13$ TeV to see how these variables can separate the three signals, namely, singlet, doublet, and triplet. The normalized distributions for z_1 and z_2 are shown in Fig. 1. Both z_1 and z_2 peak on the lower side for triplet (red lines)

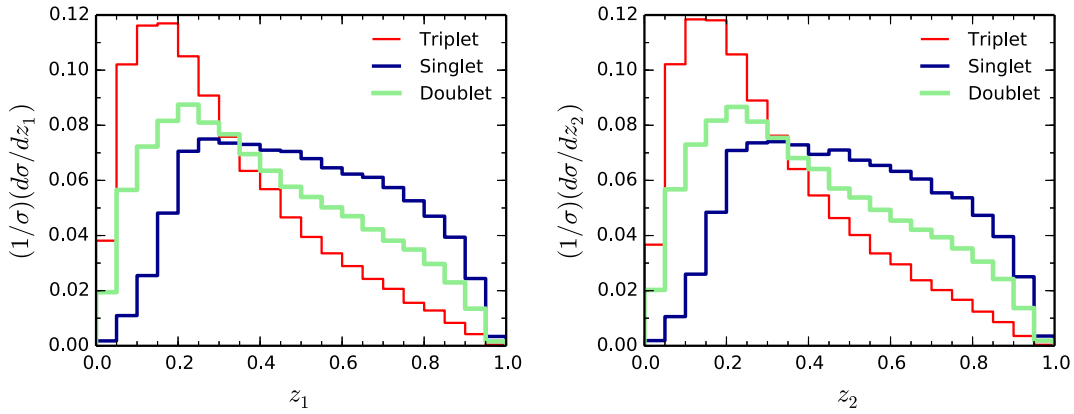

FIG. 1. Normalized distributions for the visible energy fractions z_1 and z_2 for the signals with parton-level events. See the text for further discussions.

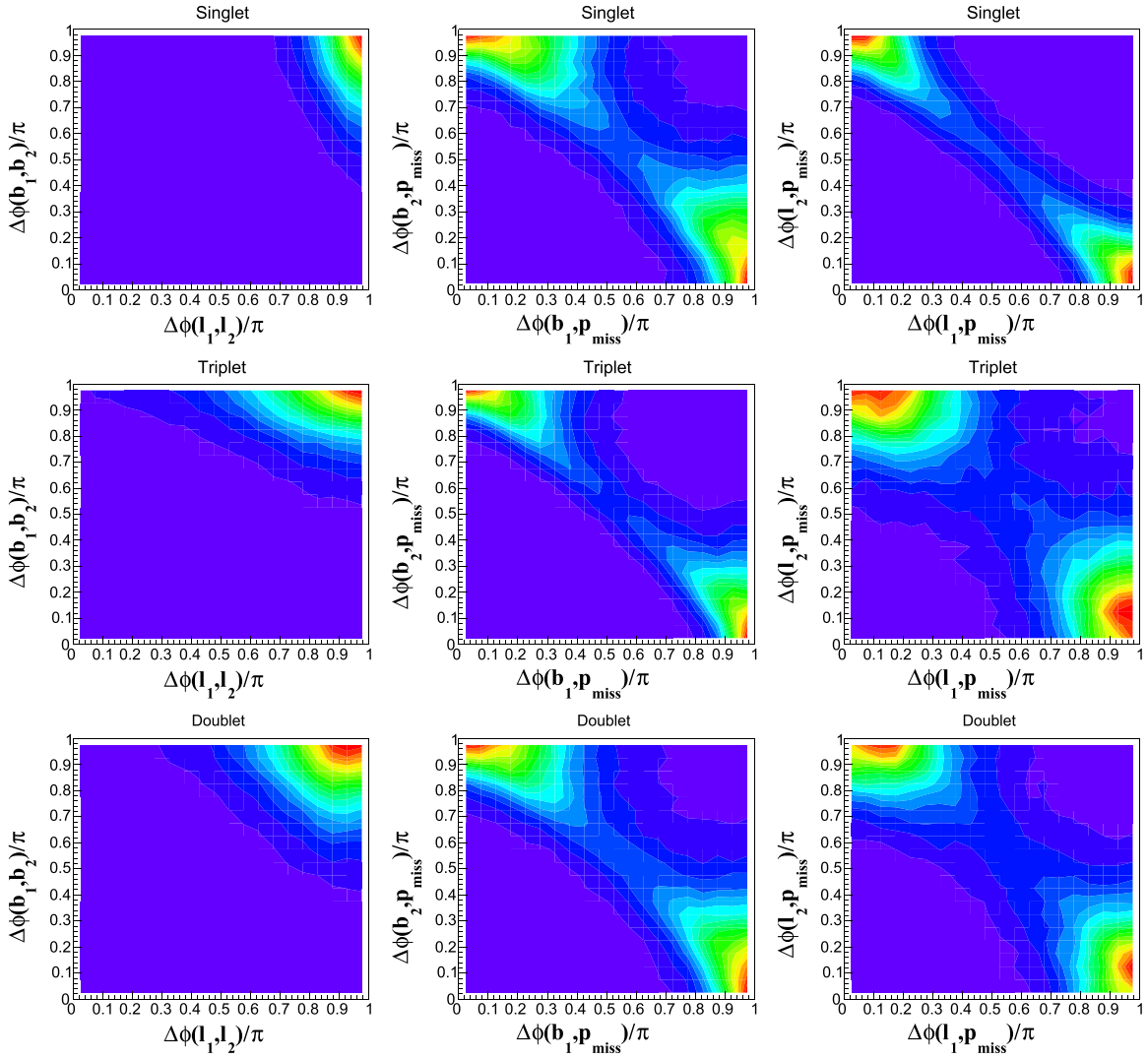

FIG. 2. Normalized distributions for the two-dimensional correlations between $\Delta\phi(l_1, l_2)$ vs $\Delta\phi(b_1, b_2)$ (left column), $\Delta\phi(b_1, p_{\rm miss})$ vs $\Delta\phi(b_2, p_{\rm miss})$ (middle column), and $\Delta\phi(l_1, p_{\rm miss})$ vs $\Delta\phi(l_2, p_{\rm miss})$ (right column) for the signals with parton-level events. The red points represent maximum density, and light blue represents the minimum density for the number of events.

as the produced top quarks are left handed in this case. This means the final-state leptons are less boosted as we go from the top rest frame to the laboratory frame, and thus z_i's peak at smaller values. For the singlet (blue lines), the variables z_i sharply drop near 0.2, having more fractional events with $z_i > 0.5$, compared to the tripet. For the doublet (green lines), however, the variables peak below $z_i = 0.5$, but the asymmetry with respect to $z_i = 0.5$ is smaller than the triplet since the doublet decay gives rise to both left-handed as well as right-handed top quarks. With realistic detector effects, the strengths of these variables might diminish, but the qualitative result would remain the same, as we will see below. We define net asymmetries for the visible energy fractions (z_i) as

$$\mathcal{A}_{z_i} = \frac{N(z_i > c_{z_i}) - N(z_i < c_{z_i})}{N_{\rm tot}}, \tag{8}$$

with $N(x > c)$ being the number of events with $x > c$ and $N_{\rm tot}$ being the total number of events. We only consider the tt production process containing the $2\ell^+$ final state and do not include the charge conjugation process because $\sigma_{\bar{t}\bar{t}}/\sigma_{tt} \approx 0.03$ owing to the small parton distribution functions (PDFs) at the LHC.

Similar to the polarization parameters, one can construct variables to capture the spin correlation between the two top quarks using the laboratory frame angular separation between the final-state particles in the transverse plane. We study two-dimensional (2D) correlations between $\Delta\phi(l_1, l_2)$ vs $\Delta\phi(b_1, b_2)$, $\Delta\phi(b_1, p_{\rm miss})$ vs $\Delta\phi(b_2, p_{\rm miss})$, and $\Delta\phi(l_1, p_{\rm miss})$ vs $\Delta\phi(l_2, p_{\rm miss})$. The normalized 2D correlations are shown in Fig. 2 with parton-level events. The correlations are not symmetric with respect to the diagonal axes, and they are different for different signals. In the first column in Fig. 2, the distributions are more peaked

in $\Delta\phi(l_1, l_2)$ compared to $\Delta\phi(b_1, b_2)$ for the singlet, while the opposite is true for the triplet. For the doublet, however, the distributions are less peaked and more symmetric around the $\Delta\phi(l_1, l_2) = \Delta\phi(b_1, b_2)$ line. This can be explained in the following way. As the two top quarks are produced from a heavy resonance, $\Delta\phi(l_1, l_2)$ and $\Delta\phi(b_1, b_2)$ are expected to peak around π in the laboratory frame due to relativistic focusing. But due to the positive polarization of top quarks from the singlet, the leptons (b quarks) are emitted primarily in the same (opposite) direction as the top-quark spin in the top rest frame. As a result, after boosting to the laboratory frame, the peak of $\Delta\phi(l_1, l_2)$ becomes sharper, while the peak of $\Delta\phi(b_1, b_2)$ becomes broader. For the triplet with negatively polarized top quarks, the opposite happens, i.e., the peak of $\Delta\phi(b_1, b_2)$ becomes sharper, while the peak of $\Delta\phi(l_1, l_2)$ becomes broader. Finally for the doublet, with a mix of positively and negatively polarized top quarks, the peaks of $\Delta\phi(l_1, l_2)$ and $\Delta\phi(b_1, b_2)$ have similar broadening.

The $\Delta\phi(l/b, p_{\rm miss})$ peak near zero and π, as shown in the second and third columns of Fig. 2. The distribution of $\Delta\phi(l/b, p_{\rm miss})$ can be explained in a way similarly to that of $\Delta\phi(l_1/b_1, l_2/b_2)$, after noting that $\bar{\nu}$ is distributed the same way as b quarks around the top-quark spin in the top rest frame. The peak of $\Delta\phi(l, p_{\rm miss})$ is sharper than that of $\Delta\phi(b, p_{\rm miss})$ for the singlet, and the opposite is truefor the triplet. For the doublet, $\Delta\phi(l, p_{\rm miss})$ and $\Delta\phi(b, p_{\rm miss})$ behave roughly in the same way. Given this, we propose the following variables based on these 2D correlations,

$$\begin{aligned} x_{lb} &= \Delta\phi(l_1, l_2)/\pi - \Delta\phi(b_1, b_2)/\pi, \\ x_{ll} &= \Delta\phi(l_1, p_{\rm miss})/\pi + \Delta\phi(l_2, p_{\rm miss})/\pi, \\ x_{bb} &= \Delta\phi(b_1, p_{\rm miss})/\pi + \Delta\phi(b_2, p_{\rm miss})/\pi, \end{aligned} \tag{9}$$

to extract the spin correlation of the two top quarks. The asymmetries for the correlations are defined as

$$\mathcal{A}_{lb} = \frac{N(x_{lb} > 0) - N(x_{lb} < 0)}{N_{\rm tot}}, \tag{10}$$

$$\mathcal{A}_{ll} = \frac{N(|x_{ll} - 1| < c_{ll}) - N(|x_{ll} - 1| > c_{ll})}{N_{\rm tot}}, \tag{11}$$

$$\mathcal{A}_{bb} = \frac{N(|x_{bb} - 1| < c_{bb}) - N(|x_{bb} - 1| > c_{bb})}{N_{\rm tot}}. \tag{12}$$

TABLE I. Values of asymmetries for the signals with parton-level events. For all the signals, we choose $\lambda = 0.003$ and $m_\phi = 1$ TeV.

	$\mathcal{A}_{z_1}$	$\mathcal{A}_{z_2}$	$\mathcal{A}_{lb}$	$\mathcal{A}_{ll}$	$\mathcal{A}_{bb}$
Singlet	0.31	0.31	0.33	0.58	0.05
Triplet	−0.36	−0.36	−0.31	0.0	0.28
Doublet	−0.03	−0.03	−0.10	0.07	0.11

Note that these $\Delta\phi$ variables are independent of pairing the leptons and the b quarks; the pairing is required only for the variables z_i.

To maximize the asymmetries defined in Eqs. (8), (10), (12), and (11), we choose $c_{z_1} = c_{z_2} \simeq 0.38$ and $c_{bb} = c_{ll} \simeq 0.14$ by observing the parton-level distributions in Figs. 1 and 2. The values of the asymmetries at parton level are listed in Table I for the three signals. It is clear that with the magnitudes and signs of the asymmetries one can easily identify and separate the signals. However, we need to extract these asymmetries with realistic detector effects, including possible backgrounds. Therefore, in the next section, we analyze the signals with detector-level events in the presence of SM backgrounds.

IV. RESULTS

In this section, we discuss how to distinguish the three types of signals in the presence of background events, with a simplified detector-level simulation. The backgrounds that can mimic our signal topology of two positively charged leptons ($2l^+$), two b jets, and missing energy are [25,32–34] $t\bar{t}W^+$, $t\bar{t}Z$, $t\bar{t}h$, $t\bar{t}W^+W^-$, W^+W^+jj, $ZZjj$, ZZW^+, and W^+W^-Z. In addition, the $t\bar{t}+$jets process, which has a large cross section, can fake our signal if the lepton charges get misidentified [35–37]. We generate the signal (singlet, doublet, and triplet) and background events in MADGRAPH5_AMC@NLOV2.7.3 [38] at leading order in QCD, without cuts on the final-state particles, and with a dynamic choice of factorization scale given by $\sum_i M_i^T/2$, where M_i^T is the transverse mass of the ith final-state particle. We use NN23LO1 [39] for the PDFs. Background events are generated in MADGRAPH5 with the final states that can give rise to $2l^+2b + \not{E}_T$ at the detector level. Events are then passed to PYTHIA8.2 [40] for showering and hadronization, followed by fast detector simulation in DELPHES3.4.2 [41]. Events are selected at detector level with at least two b-tagged jets, two positively charged leptons ($2l^+$), and missing transverse energy with the following selection-level cuts:

$$\begin{aligned} &p_T(l) > 10\ \text{GeV}, \quad p_T(b) > 20\ \text{GeV}, \quad \not{E}_T > 10\ \text{GeV}, \\ &\Delta R(b, b) > 0.5, \quad \Delta R(b, l) > 0.4, \quad \Delta R(l, l) > 0.4, \\ &|\eta_b| < 2.5, \quad |\eta_l| < 2.5. \end{aligned} \tag{13}$$

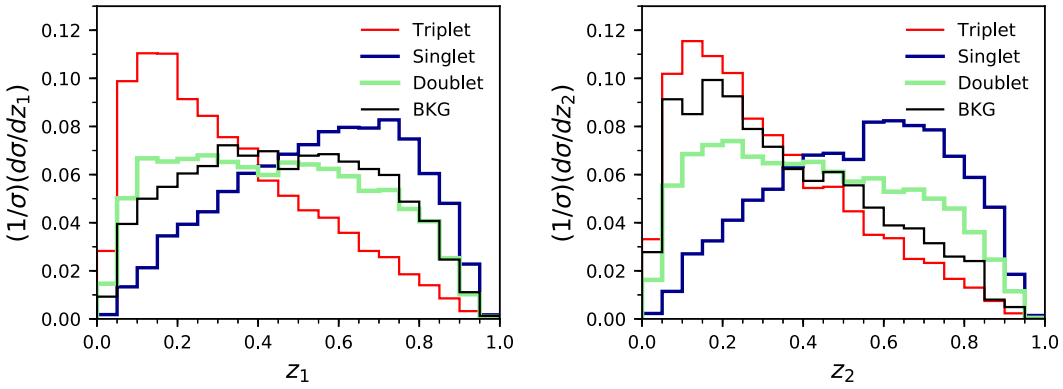

FIG. 3. Normalized distributions for the visible energy fractions z_1 and z_2 for the signals and background at DELPHES level with selection cuts as in Eq. (13).

With the selected background (BKG) and signal events, we study the one-dimensional and two-dimensional normalized distributions for the variables (z_i and $\Delta\phi$ correlation, respectively) that we introduced in the previous section. These are shown in Figs. 3 (z_i) and 4 ($\Delta\phi$). The qualitative features of the distributions at the detector level remain the same as the parton-level distributions studied in the previous section. The z_i distributions make clear distinctions between the singlet and triplet peaking in the right and left, respectively. Distributions are roughly symmetric around $z_i = 0.5$ for the doublet. For the BKG, the z_1 distribution is symmetric around $z_1 = 0.5$ as well, while the z_2 distribution is asymmetric. In the case of all three signal benchmarks, the distributions for the z_1 and z_2 are identical, owing to the similar kinematics. However, this not true for the background because the paired lepton and b quark do not necessarily originate from a top quark. Additionally, z_2 peaks at lower values, owing to the p_T ordering of leptons. In the 2D $\Delta\phi$ distributions, the background events are distributed quite differently than the signals. Therefore, it is possible to distinguish the signals based on these distributions, even with the detector-level events. However, the total cross section for the background is larger than that for the signal, and therefore we now discuss some kinematic cuts that are needed to reduce backgrounds and increase the signal sensitivity.

We study various kinematic distributions, such as the transverse momenta (p_T) of the final-state particles, total hadronic energy (H_T), and visible mass ($m_{l_1^+ l_2^+ b_1 b_2}$). We find that visible mass, the normalized distribution shown in Fig. 5, can be used to suppress the background and enhance the significance of all three signals. In particular, a cut on the visible mass of

$$m_{l_1^+ l_2^+ b_1 b_2} > 430 \text{ GeV} \tag{14}$$

maximizes the signal significance. The signal and background processes are summarized in Table II, showing their cross sections at the generation level and the expected number of events for an integrated luminosity of $\mathcal{L} = 300$ fb^{-1} after the visible mass cut. The total number of background events is expected to be 208 in the $2l^+2b\not{E}_T$ final state. The signal significance expected for the three signals is given in Table III for integrated luminosities of $\mathcal{L} = 150$ fb^{-1} (currently available), 300 fb^{-1} (next phase of LHC), and 3000 fb^{-1} (high-luminosity phase). We calculate the signal significance [42] using

$$S = \sqrt{2\left[(s+b)\log\left(1+\frac{s}{b}\right) - s\right]}, \tag{15}$$

where s and b stand for the total number of signal and background events surviving after cuts. For the chosen coupling of $\lambda = 0.003$ and $m_\phi = 1$ TeV, the significance for the triple and doublet signals are higher than the singlet signal. A luminosity of about 1300 fb^{-1} is required for discovery of singlet, whereas the doublet and triplet can be discovered with about 790 and 930 fb^{-1} of luminosity, respectively with 5σ significance.

Having discussed the discovery potential for the signals, we now turn to our primary goal of this analysis, which is to distinguish among the three signals with the help of the observables discussed in Sec. III. To this end, we first calculate the asymmetries for all the variables and summarize them in Table IV for all three signals and backgrounds separately, as well as signals in the presence of backgrounds. The numbers in the first three rows show that all three signals can be identified by looking at the value and the sign of the five asymmetries. However, these asymmetries are affected by the background events, as shown in the last three rows. We calculate the differences between any two signals in the presence of backgrounds using all five asymmetries, given in Table IV, in terms of the χ^2 function

$$\chi^2 = \sum_i \left| \frac{\mathcal{A}_i(\text{Signal1} + \text{BKG}) - \mathcal{A}_i(\text{Signal2} + \text{BKG})}{\delta\mathcal{A}_i(\text{BKG})} \right|^2. \tag{16}$$

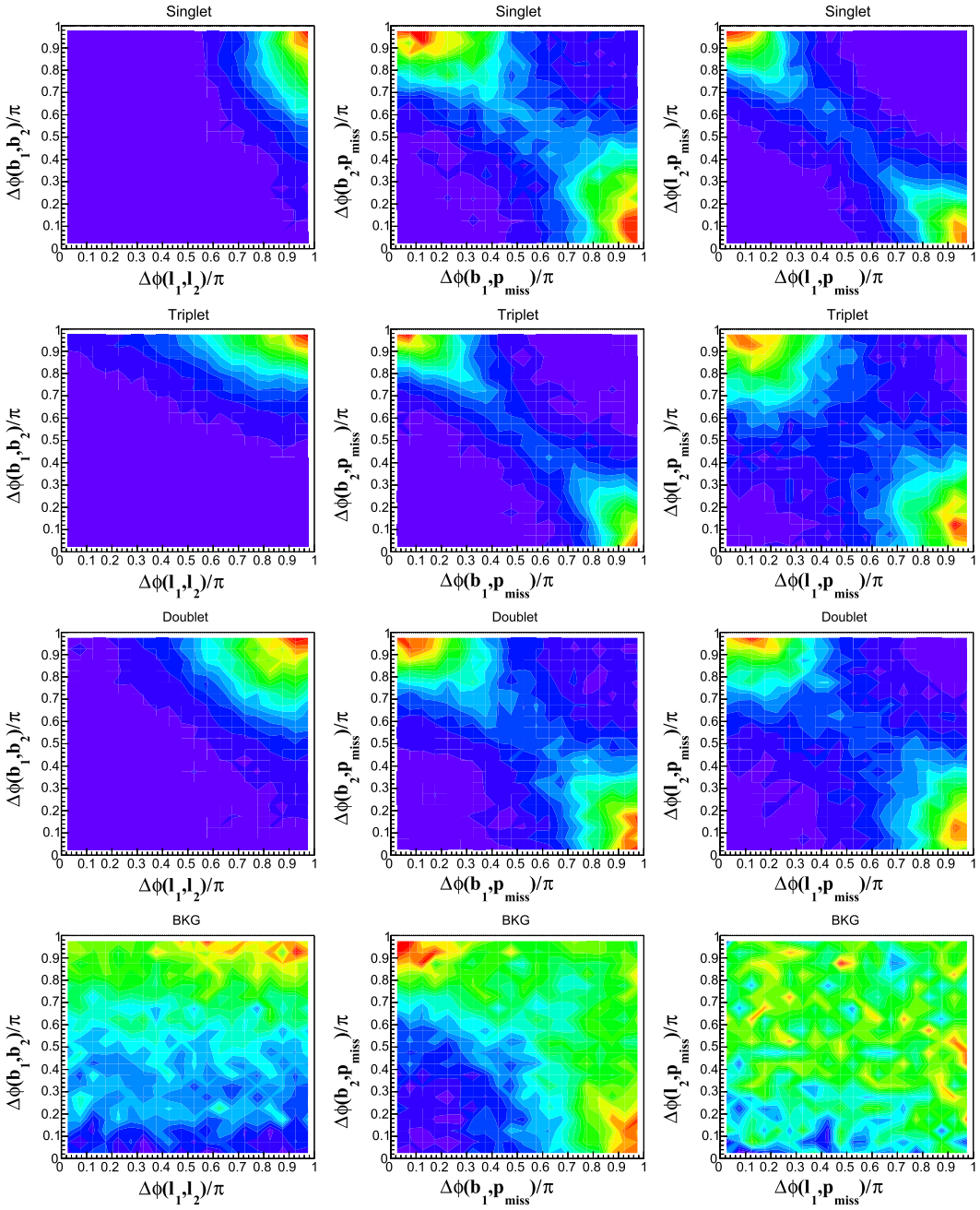

FIG. 4. Normalized distributions for the two-dimensional correlations between $\Delta\phi(l_1, l_2)$ vs. $\Delta\phi(b_1, b_2)$ (left-column), $\Delta\phi(b_1, p_{\rm miss})$ vs. $\Delta\phi(b_2, p_{\rm miss})$ (middle-column), and $\Delta\phi(l_1, p_{\rm miss})$ vs. $\Delta\phi(l_2, p_{\rm miss})$ (right-column) for the signals and background at DELPHES level with selection cuts in Eq. (13). The color description is the same as in Fig. 2.

Here, $\delta\mathcal{A}_i(\mathrm{BKG}) = \sqrt{\frac{1-\mathcal{A}_i^2(\mathrm{BKG})}{\mathcal{L}\sigma(\mathrm{BKG})}}$ is the statistical uncertainty due to the SM backgrounds with $\sigma(\mathrm{BKG})$ being the total background cross section. Signal_j ($j = 1, 2$) denote any two among the singlet, doublet, and triplet signals. We estimate the luminosity required for 2σ, 3σ, and 5σ C.L. separability among the signals using the above χ^2 functions and quote them in Table V. The singlet and the triplet are quite different since the former (latter) decays only into right-chiral (left-chiral) top quarks; a luminosity of about 628 fb^{-1} is required to achieve separability at 5σ C.L., although neither of them can be discovered for that luminosity with the expected number of events (see Table III). On the other hand, we require about 2842 and 2061 fb^{-1} of luminosity for 5σ separation between the singlet versus doublet and doublet versus triplet, respectively, as the two top quarks have both chiralities originating from the doublet. Thus, to make distinctions between the signals involving the doublet, we need higher luminosity than what is required to discover them.

TABLE II. The signal and the background cross sections and the expected number of events for an integrated luminosity of $\mathcal{L} = 300$ fb^{-1} with selection cuts in Eq. (13) as well as the visible mass cut in Eq. (14). The contents in the parentheses of the first column correspond to the final states contributing to the $2l^+2b\not{E}_T$ final state. For all signals, we choose $\lambda = 0.003$ and $m_\phi = 1$ TeV.

Process (generated up to)	Cross section (fb)	Efficiency (ϵ)	Expected events ($2l^+2b\not{E}_T$)
Singlet: $tt(2l^+2b\not{E}_T)$	1.121	10.62%	35.7
Doublet: $tt(2l^+2b\not{E}_T)$	1.348	11.40%	46.1
Triplet: $tt(2l^+2b\not{E}_T)$	1.166	12.06%	42.2
B1: $t\bar{t}W^+(2l^+2b2j\not{E}_T)$	9.2	3.75%	103.5
B2: $t\bar{t}Z(t \to l^+b\not{E}_T, \bar{t} \to \bar{b}jj + \bar{b}l^-\not{E}_T, Z \to 2l)$	8.056	1.76%	42.6
B3: $t\bar{t} + jj(t/\bar{t} \to l^+/l^-)$	29482.0	4.7×10^{-4}%	41.6
B4: $t\bar{t}h + jj(t/\bar{t} \to l^+/l^-, h \to \text{all})$	23.68	0.14%	10.3
B5: $t\bar{t}W^+W^-(t/W^+ \to l^+, \bar{t}/W^- \to \text{all})$	0.398	4.94%	5.9
B6: $W^+W^+jj(2l^+2j\not{E}_T)$	8.967	0.11%	2.9
B7: $ZZjj(4l2j)$	12.69	0.02%	0.8
B8: $ZZW^+(4ljj + 3ljj\not{E}_T)$	0.4	0.17%	0.2
B9: $W^+W^-Z(3l2j\not{E}_T)$	1.61	$\leq 10^{-3}$%	0
Total background			207.8

TABLE III. Signal significance using only the total number of events with integrated luminosities of $\mathcal{L} = 150$, 300, and 3000 fb^{-1} with selection cuts in Eq. (13) as well as the visible mass cut in Eq. (14). For all the signals, we choose $\lambda = 0.003$ and $m_\phi = 1$ TeV.

Signal	150 fb^{-1}	300 fb^{-1}	3000 fb^{-1}	$\mathcal{L}$ for 5σ C.L.
Singlet	1.70	2.40	7.59	$\simeq$1300 fb^{-1}
Doublet	2.18	3.09	9.77	$\simeq$790 fb^{-1}
Triplet	2.01	2.84	8.97	$\simeq$930 fb^{-1}

TABLE IV. Values of asymmetries for the signals along with the backgrounds with selection cuts in Eq. (13) as well as the visible mass cut in Eq. (14). For all the signals, we choose $\lambda = 0.003$ and $m_\phi = 1$ TeV.

	$\mathcal{A}_{z_1}$	$\mathcal{A}_{z_2}$	$\mathcal{A}_{lb}$	$\mathcal{A}_{ll}$	$\mathcal{A}_{bb}$
Singlet	0.52	0.49	0.28	0.35	−0.04
Doublet	0.13	0.09	−0.12	−0.03	0.08
Triplet	−0.27	−0.32	−0.36	−0.09	0.32
BKG	0.14	−0.28	−0.31	−0.50	−0.25
Singlet + BKG	0.19	−0.16	−0.22	−0.38	−0.21
Doublet + BKG	0.14	−0.21	−0.27	−0.42	−0.19
Triplet + BKG	0.07	−0.28	−0.31	−0.43	−0.15

V. CONCLUSION

In this work, we have discussed how to measure the electroweak quantum numbers of BSM color sextet scalar and vector particles. While all the sextet particles that we consider decay into a *like-sign* top-quark pair, the top quarks have identical chirality for the two sextet scalars and opposite chirality for the sextet vector. Furthermore, one of the scalars gives rise to left-handed top quarks, while the other decays to right-handed ones. These features can be captured by several kinematic variables that rely only on visible final states. One such variable is the well known visible energy fraction (z_i) of final-state leptons, Eq. (2). Here, we construct three additional variables, defined in Eq. (9), that depend on the angular correlation between the final-state leptons and b jets. All of these variables are sensitive to the polarization of the top quarks and in a combined fashion can distinguish among the three possible sextet states.

Through a parton-level analysis, we first demonstrate the utility of the visible energy fraction variables and the angular correlation variables. We study their distributions in Figs. 1 and 2 and compute a set of asymmetries in Table I to identify the differences among the three signals. These show that the asymmetries can fully distinguish as well as identify the quantum numbers of the sextet states, in principle.

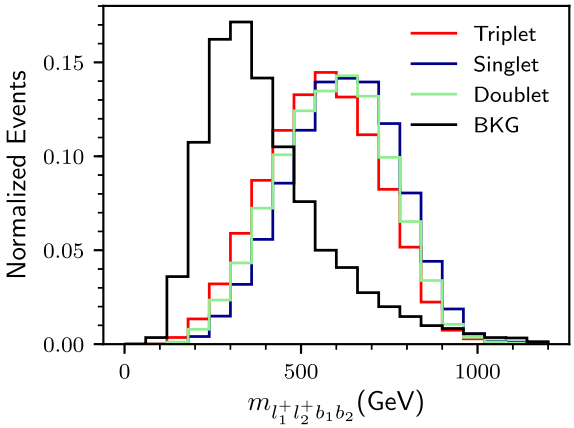

FIG. 5. Normalized distributions for the visible mass with selection cuts in Eq. (13). For all signals, we choose $\lambda = 0.003$ and $m_\phi = 1$ TeV.

TABLE V. Luminosity ($\mathcal{L}$) required to distinguish between the models at 2σ, 3σ, and 5σ C.L. based on the asymmetries with selection cuts in Eq. (13) as well as the visible mass cut in Eq. (14). We choose $\lambda = 0.003$ and $m_\phi = 1$ TeV for all the signals.

	Luminosity required (fb^{-1})		
Signal_1 vs Signal_2	2σ C.L.	3σ C.L.	5σ C.L.
Singlet vs doublet	455	1023	2842
Singlet vs triplet	100	226	628
Doublet vs triplet	330	742	2061

We then implement a simplified detector-level simulation, taking into account possible SM backgrounds, to verify how well we can differentiate among the three types of signals. We find that, while the three signals can be distinguished among themselves even at the detector level, the inclusion of SM background reduces the difference among the signals. Nonetheless, with sufficient statistics within the reach of the high-luminosity phase of the LHC, the three types of signals can still be distinguished, as demonstrated in Table V. We find higher luminosities are required to make all these distinctions than the luminosities required to discover them. To summarize, if discovered at the LHC, it is possible to measure the electroweak quantum numbers of BSM color sextet particles using top-quark polarization and spin correlation observables.

ACKNOWLEDGMENTS

S. K. is supported in part by the U.S. National Science Foundation (NSF) Grant No. PHY-1915314 and the DOE Contract No. DE-AC02-05CH11231. S. K. thanks IISER Kolkata for hospitality during various stages of this work. R. R. would like to acknowledge support from the Department of Atomic Energy, Government of India, for the Regional Centre for Accelerator-based Particle Physics (RECAPP), Harish Chandra Research Institute.

[1] R. L. Workman *et al.* (Particle Data Group Collaboration), Review of particle physics, Prog. Theor. Exp. Phys. **2022**, 083C01 (2022).
[2] E. Ma, M. Raidal, and U. Sarkar, Probing the exotic particle content beyond the standard model, Eur. Phys. J. C **8**, 301 (1999).
[3] E. Del Nobile, R. Franceschini, D. Pappadopulo, and A. Strumia, Minimal matter at the large hadron collider, Nucl. Phys. **B826**, 217 (2010).
[4] J. M. Arnold, B. Fornal, and M. B. Wise, Simplified models with baryon number violation but no proton decay, Phys. Rev. D **87**, 075004 (2013).
[5] Z. Chacko and R. N. Mohapatra, Supersymmetric SU(2)-L x SU(2)-R x SU(4)-c and observable neutron—anti-neutron oscillation, Phys. Rev. D **59**, 055004 (1999).
[6] O. Cakir and M. Sahin, Resonant production of diquarks at high energy pp, ep and e^+e^- colliders, Phys. Rev. D **72**, 115011 (2005).
[7] R. N. Mohapatra, N. Okada, and H.-B. Yu, Diquark Higgs at LHC, Phys. Rev. D **77**, 011701 (2008).
[8] C.-R. Chen, W. Klemm, V. Rentala, and K. Wang, Color sextet scalars at the CERN large hadron collider, Phys. Rev. D **79**, 054002 (2009).
[9] C. W. Bauer, Z. Ligeti, M. Schmaltz, J. Thaler, and D. G. E. Walker, Supermodels for early LHC, Phys. Lett. B **690**, 280 (2010).
[10] T. Han, I. Lewis, and T. McElmurry, QCD corrections to scalar diquark production at hadron colliders, J. High Energy Phys. 01 (2010) 123.
[11] J. M. Arnold, M. Pospelov, M. Trott, and M. B. Wise, Scalar representations and minimal flavor violation, J. High Energy Phys. 01 (2010) 073.
[12] H. Zhang, E. L. Berger, Q.-H. Cao, C.-R. Chen, and G. Shaughnessy, Color sextet vector bosons and same-sign top quark pairs at the LHC, Phys. Lett. B **696**, 68 (2011).
[13] T. Han, I. Lewis, and Z. Liu, Colored resonant signals at the LHC: Largest rate and simplest topology, J. High Energy Phys. 12 (2010) 085.
[14] E. L. Berger, Q.-H. Cao, C.-R. Chen, G. Shaughnessy, and H. Zhang, Color Sextet Scalars in Early LHC Experiments, Phys. Rev. Lett. **105**, 181802 (2010).
[15] G. F. Giudice, B. Gripaios, and R. Sundrum, Flavourful production at hadron colliders, J. High Energy Phys. 08 (2011) 055.
[16] R. S. Chivukula, P. Ittisamai, K. Mohan, and E. H. Simmons, Color discriminant variable and scalar diquarks at the LHC, Phys. Rev. D **92**, 075020 (2015).
[17] C. G. Lester and D. J. Summers, Measuring masses of semiinvisibly decaying particles pair produced at hadron colliders, Phys. Lett. B **463**, 99 (1999).
[18] A. Barr, C. Lester, and P. Stephens, m(T2): The truth behind the glamour, J. Phys. G **29**, 2343 (2003).
[19] W. S. Cho, K. Choi, Y. G. Kim, and C. B. Park, M(T2)-assisted on-shell reconstruction of missing momenta and its application to spin measurement at the LHC, Phys. Rev. D **79**, 031701 (2009).
[20] D. Guadagnoli and C. B. Park, M_{T2}-reconstructed invisible momenta as spin analizers, and an application to top polarization, J. High Energy Phys. 01 (2014) 030.
[21] J. Shelton, Polarized tops from new physics: Signals and observables, Phys. Rev. D **79**, 014032 (2009).
[22] E. L. Berger, Q.-H. Cao, J.-H. Yu, and H. Zhang, Measuring Top Quark Polarization in Top Pair plus Missing Energy Events, Phys. Rev. Lett. **109**, 152004 (2012).

[23] C.-H. Chen, Impact of colored scalars on D(0)—anti-D(0) mixing in diquark models, Phys. Lett. B **680**, 133 (2009).
[24] R. Aaij *et al.* (LHCb Collaboration), Observation of the Mass Difference Between Neutral Charm-Meson Eigenstates, Phys. Rev. Lett. **127**, 111801 (2021).
[25] A. M. Sirunyan *et al.* (CMS Collaboration), Search for physics beyond the standard model in events with two leptons of same sign, missing transverse momentum, and jets in proton–proton collisions at $\sqrt{s} = 13$ TeV, Eur. Phys. J. C **77**, 578 (2017).
[26] W. Bernreuther and A. Brandenburg, Signatures of Higgs sector *CP* violation in top quark pair production at proton proton supercolliders, Phys. Lett. B **314**, 104 (1993).
[27] F. Boudjema and R. K. Singh, A model independent spin analysis of fundamental particles using azimuthal asymmetries, J. High Energy Phys. 07 (2009) 028.
[28] V. Khachatryan *et al.* (CMS Collaboration), Measurement of the differential cross section for top quark pair production in pp collisions at $\sqrt{s} = 8$ TeV, Eur. Phys. J. C **75**, 542 (2015).
[29] A. M. Sirunyan *et al.* (CMS Collaboration), Measurements of $t\bar{t}$ differential cross sections in proton-proton collisions at $\sqrt{s} = 13$ TeV using events containing two leptons, J. High Energy Phys. 02 (2019) 149.
[30] A. M. Sirunyan *et al.* (CMS Collaboration), Measurement of the top quark polarization and $t\bar{t}$ spin correlations using dilepton final states in proton-proton collisions at $\sqrt{s} = 13$ TeV, Phys. Rev. D **100**, 072002 (2019).
[31] R. Rahaman, On two-body and three-body spin correlations in leptonic $t\bar{t}Z$ production and anomalous couplings at the LHC, J. High Energy Phys. 02 (2023) 077.
[32] T. Modak, Implications of the heavy Higgs induced single-top, same-sign top and triple-top productions at the LHC,
[33] O. M. Ozsimsek, V. Ari, and O. Cakir, Studying same-sign top pair production in flavor changing scalar models at the HL-LHC, Adv. High Energy Phys. **2022**, 4299254 (2022).
[34] W.-S. Hou, T.-H. Hsu, and T. Modak, Constraining the $t \to u$ flavor changing neutral Higgs coupling at the LHC, Phys. Rev. D **102**, 055006 (2020).
[35] M. Aaboud *et al.* (ATLAS Collaboration), Search for new phenomena in events with same-charge leptons and b-jets in pp collisions at $\sqrt{s} = 13$ TeV with the ATLAS detector, J. High Energy Phys. 12 (2018) 039.
[36] ATLAS Collaboration, Search for supersymmetry with two same-sign leptons or three leptons using 13.2 fb^{-1} of $\sqrt{s} = 13$ TeV pp collision data collected by the ATLAS detector, http://cds.cern.ch/record/2205745.
[37] E. Alvarez, D. A. Faroughy, J. F. Kamenik, R. Morales, and A. Szynkman, Four tops for LHC, Nucl. Phys. **B15**, 19 (2017).
[38] J. Alwall, R. Frederix, S. Frixione, V. Hirschi, F. Maltoni, O. Mattelaer, H. S. Shao, T. Stelzer, P. Torrielli, and M. Zaro, The automated computation of tree-level and next-to-leading order differential cross sections, and their matching to parton shower simulations, J. High Energy Phys. 07 (2014) 079.
[39] R. D. Ball *et al.* (NNPDF Collaboration), Parton distributions for the LHC Run II, J. High Energy Phys. 04 (2015) 040.
[40] T. Sjöstrand, S. Ask, J. R. Christiansen, R. Corke, N. Desai, P. Ilten, S. Mrenna, S. Prestel, C. O. Rasmussen, and P. Z. Skands, An introduction to PYTHIA8.2, Comput. Phys. Commun. **191**, 159 (2015).
[41] J. de Favereau, C. Delaere, P. Demin, A. Giammanco, V. Lemaître, A. Mertens, and M. Selvaggi (DELPHES 3 Collaboration), DELPHES 3, A modular framework for fast simulation of a generic collider experiment, J. High Energy Phys. 02 (2014) 057.
[42] G. Cowan, K. Cranmer, E. Gross, and O. Vitells, Asymptotic formulae for likelihood-based tests of new physics, Eur. Phys. J. C **71**, 1554 (2011); **73**, 2501(E) (2013).